Macromolecules

Article

pubs.acs.org/Macromolecules

Confined Dynamics of Grafted Polymer Chains in Solutions of Linear Polymer

Ryan Poling-Skutvik,[†] Katy N. Olafson,[†] Suresh Narayanan,[‡] Laura Stingaciu,[§] Antonio Faraone,[∥] Jacinta C. Conrad,*[,†] and Ramanan Krishnamoorti*[,†]

[†]Department of Chemical and Biomolecular Engineering, University of Houston, Houston, Texas 77204, United States

[‡]Advanced Photon Source, Argonne National Laboratory, Argonne, Illinois 60439, United States

[§]Jülich Centre for Neutron Science JCNS, Forschungszentrum Jülich GmbH, Outstation at SNS, Oak Ridge National Laboratory, Oak Ridge, Tennessee 37831, United States

[∥]National Institute of Standards and Technology Center for Neutron Research, Gaithersburg, Maryland 20899, United States

Supporting Information

ABSTRACT: We measure the dynamics of high molecular weight polystyrene grafted to silica nanoparticles dispersed in semidilute solutions of linear polymer. Structurally, the linear free chains do not penetrate the grafted corona but increase the osmotic pressure of the solution, collapsing the grafted polymer and leading to eventual aggregation of the grafted particles at high matrix concentrations. Dynamically, the relaxations of the grafted polymer are controlled by the solvent viscosity according to the Zimm model on short time scales. On longer time scales, the grafted chains are confined by neighboring grafted chains, preventing full relaxation over the experimental time scale. Adding free linear polymer to the solution does not affect the initial Zimm relaxations of the grafted polymer but does increase the confinement of the grafted chains. Our results elucidate the physics underlying the slow relaxations of grafted polymer.

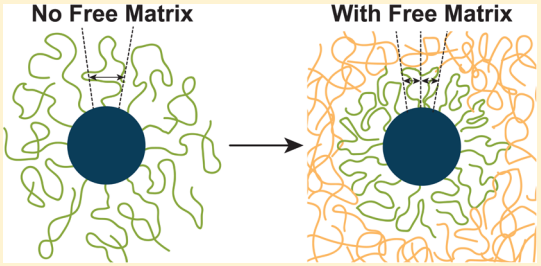

INTRODUCTION

Polymers grafted to surfaces modify the structure of and interactions between surfaces to enhance nanoparticle dispersion in polymer composites,[1] improve biocompatibility for targeted drug delivery,[2] and serve as flexible sensors.[3] Controlling these processes requires an understanding of the dynamics of polymer brushes in and out of equilibrium.[4] The dynamics of grafted polymer depends on grafting density σ and surface curvature and is distinct from that of free polymer. In the absence of hydrodynamic interactions, free polymer chains with N repeat units relax according to the Rouse model with a relaxation time $\tau \sim N^2$ and a mean-squared displacement that scales as $\langle \Delta r^2 \rangle \sim t^{\alpha}$ with $\alpha = 1/2$.[5] When hydrodynamic interactions dominate, free polymers relax according to the Zimm model with $\tau \sim N^{3\nu}$ and $\alpha = 2/3$, where $\nu = 0.588$ is the inverse of the fractal dimension for a polymer in a good solvent.[5] For polymers grafted to a surface, however, interactions between the particle and polymer or between neighboring chains cannot be neglected. These physical constraints cause the relaxation times of grafted polymers to deviate from standard Zimm and Rouse predictions, scaling as $\tau \sim N^3$.[6,7] Additionally, the intrachain relaxations no longer follow simple exponential decays for polymers grafted to planar[8−12] and spherical[4] surfaces suspended in solvent.

The effects of interactions on polymers grafted to surfaces are expected to become even more pronounced in a crowded environment, such as in a polymer solution or melt, biological tissues, or confined porous media. These crowded environments lead to fascinating structural changes, notably in polymer nanocomposites[13−18] and in solutions of star and linear polymers.[19−23] For composites in which the grafted and matrix polymer are chemically similar, the dispersion of polymer grafted nanoparticles is controlled by the entropy of mixing.[13] Tuning the grafting density and molecular weight ratio can lead to a multitude of structural morphologies, including well-dispersed particles, strings, clusters, and full phase separation.[13,15] Well-dispersed particles require high grafting density and a large ratio of grafted molecular weight to matrix molecular weight.[15] Strings of particles form at high molecular weight ratios with low grafting densities, clusters form at low molecular weight ratios and low grafting densities, and full phase separation occurs at high grafting densities and low molecular weight ratios. In contrast to the entropic dewetting of grafted particles in a polymer melt, the phase behavior of star polymers in solutions of linear polymers is controlled by the osmotic pressure of the solution.[19,20] When the free polymer and star polymer are comparably sized, the free chains increase the osmotic pressure of the solution to compress the star polymers. These interactions lead to clustering and aggregation of the star polymers at high matrix concentrations and high free

Received: June 12, 2017
Revised: August 3, 2017
Published: September 11, 2017

DOI: 10.1021/acs.macromol.7b01245
Macromolecules 2017, 50, 7372−7379

chain molecular weights.[23] Depletion interactions increase in strength with increasing size of the linear polymer until the linear polymer is much larger than the star polymer, at which point the assumptions underlying the depletion model break down.[24] Conversely, free linear chains that are much smaller than the star polymers can easily penetrate them, leading to very weak interactions.[21] The effect of these structural changes on the dynamics of grafted polymer remains poorly understood, due in part to the difficulty of isolating the dynamics of the grafted chains over relevant time and length scales.

Here, we investigate the dynamics of polymer grafted on nanoparticles dispersed in solutions of chemically similar linear polymer crowders. Similar to mixtures of star and linear polymers, the linear polymer does not penetrate the grafted corona of the nanoparticles. Instead, the free chains compress the grafted layer by increasing the osmotic pressure, leading to the eventual aggregation of the nanoparticles at high matrix concentration. Using neutron spin echo spectroscopy and partial deuterium labeling of the linear chains, we measure the dynamics of the grafted chains under osmotic compression in the solutions of linear polymer. At short times, the dynamics of the grafted polymer chains follow the Zimm model, in which the solvent viscosity and hydrodynamic interactions control the polymer relaxations. At long times, however, the grafted polymer is confined by neighboring chains with a confinement length that agrees with the grafting density at the particle surface. When the grafted chains are compressed, the confining length scale decreases due to an increase in the local effective grafting density. Our work elucidates the origins of slow relaxations of grafted brushes via confinement by neighboring chains and the effect of crowding agents on the structure and dynamics of the grafted nanoparticles.

MATERIALS AND METHODS

"Grafting-To" Procedure. We use a "grafting-to" approach to covalently graft high molecular weight polystyrene chains onto silica nanoparticles (Figure 1a).[25−27] First, we dissolve 5 g of amine-terminated polystyrene of weight-averaged molecular weight M_w = 355 kDa (Polymer Source, Inc.,[a] M_w/M_n = 1.18, where M_n is the number-averaged molecular weight, radius of gyration in dilute solution $R_{g,0} \approx$ 21 nm[28]) in 600 mL of tetrahydrofuran (THF). After the polymer is fully dissolved, we add (3-glycidoxypropyl)trimethoxysilane (GPTS, Gelest, Inc., >97%) in excess and let react overnight under reflux at 65 °C while stirring. The majority of THF is removed using a rotary evaporator, and the silanized polystyrene is then precipitated by dropwise addition into excess cold methanol. The silane-functionalized polymer (GPTS-PS) is dried under vacuum at room temperature overnight, redissolved in THF, and reprecipitated in methanol to remove excess GPTS before a final drying under vacuum.

In the second step of the grafting procedure, we dissolve 5 g of GPTS-PS in 500 mL of 2-butanone. After the polymer is fully dissolved, we add 5.5 mL of the particle stock solution MEK-ST-L (Nissan Chemical America, ≈30 wt % silica in 2-butanone, R = 24 nm with a log-normal polydispersity of 0.28) and let react under reflux at 90 °C overnight. The polymer-grafted nanoparticles (GPTS-PS-SiO_2) are then precipitated into methanol and dried under vacuum overnight. Any nonfunctionalized silica particles remain stable in methanol and are removed by repeated cycles of washing with methanol and decanting. We verify the success of the grafting procedure using Fourier transform infrared spectroscopy (FTIR) and determine the grafting density σ = 0.054 ± 0.015 chains/nm^2 using thermal gravimetric analysis (TGA) (Supporting Information). This grafting density corresponds to ≈400 chains per particle.

Small-Angle Neutron Scattering. We conducted small-angle neutron scattering (SANS) measurements over a wavevector range 0.001 Å^{-1} < Q < 0.5 Å^{-1} at the NG7 beamline at the Center for Neutron Research, National Institute of Standards and Technology. The raw SANS data are corrected for detector sensitivity, empty cell scattering, and blocked beam scattering and normalized to absolute intensity $I_{total}(Q)$ using IgorPro.[29] Incoherent scattering intensity $I_{incoh}(Q)$ is determined by linear fits to $I_{total}(Q)Q^4$ vs Q^4 and subtracted from the absolute scattering to generate coherent scattering curves $I_{coh}(Q) = I_{total}(Q) - I_{incoh}(Q)$.

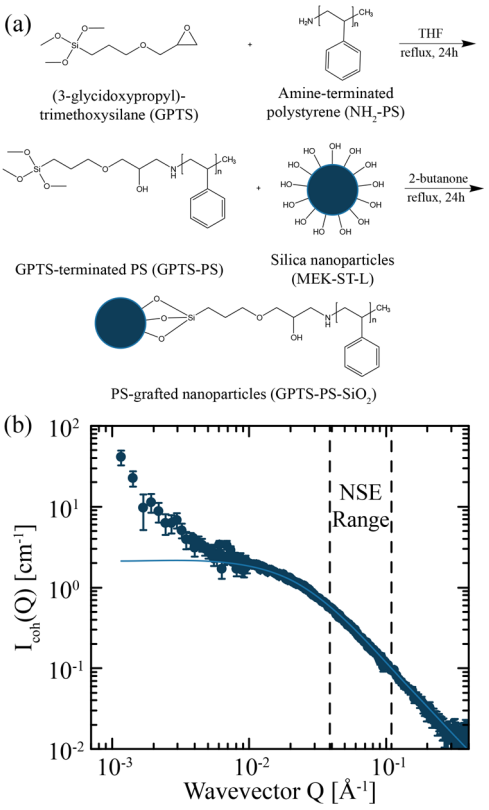

Figure 1. (a) Scheme for synthesis of polystyrene-grafted silica nanoparticles using a "grafting-to" approach. GPTS reacts with NH_2-PS under reflux to form silanized PS. Silanized PS then binds to silica nanoparticles to form polystyrene-grafted silica nanoparticles. (b) Coherent neutron scattering intensity $I_{coh}(Q)$ as a function of wavevector Q for polymer-grafted nanoparticles dispersed in d_5-2-butanone at ϕ = 0.05 and T = 25 °C. Solid curve represents best fit to a Lorentzian. Dashed lines indicate region over which NSE experiments are performed.

Small-Angle X-ray Scattering. We conduct small-angle X-ray scattering (SAXS) measurements over a wavevector range 0.0019 Å^{-1} < Q < 0.012 Å^{-1} at the X-ray photon correlation spectroscopy beamline 8-ID-I at the Advanced Photon Source, Argonne National Laboratory (ANL). The solutions are loaded into 1 mm i.d. boron-rich quartz capillary tubes (Charles-Supper) and sealed with wax to prevent evaporation. We supplement the low-Q SAXS data collected at ANL by additional SAXS measurements over a wavevector range 0.007 Å^{-1} < Q < 0.3 Å^{-1} on a Rigaku S-MAX3000 beamline at the University of Houston (UH).

Atomic Force Microscopy. For atomic force microscopy (AFM) measurements, we coat a thin coating of polymer solution over a silicon wafer, let the solvent evaporate (evaporation time <5 s), and store under vacuum overnight. We cannot spin-coat the solutions due to their high viscosity. AFM images are obtained using a Multimode atomic force microscope (Nanoscope IV) from Digital Instruments using a gold-coated silicon nitride tip (TR800PSA, Asylum Research, spring constant 0.1 N/m, tip radius 20 ± 5 nm). Images were collected in contact mode in air with a scan rate of 1 Hz and 256 scan lines over a 2 μm × 2 μm area. To achieve sufficient statistics, we collect 16

DOI: 10.1021/acs.macromol.7b01245
Macromolecules 2017, 50, 7372−7379

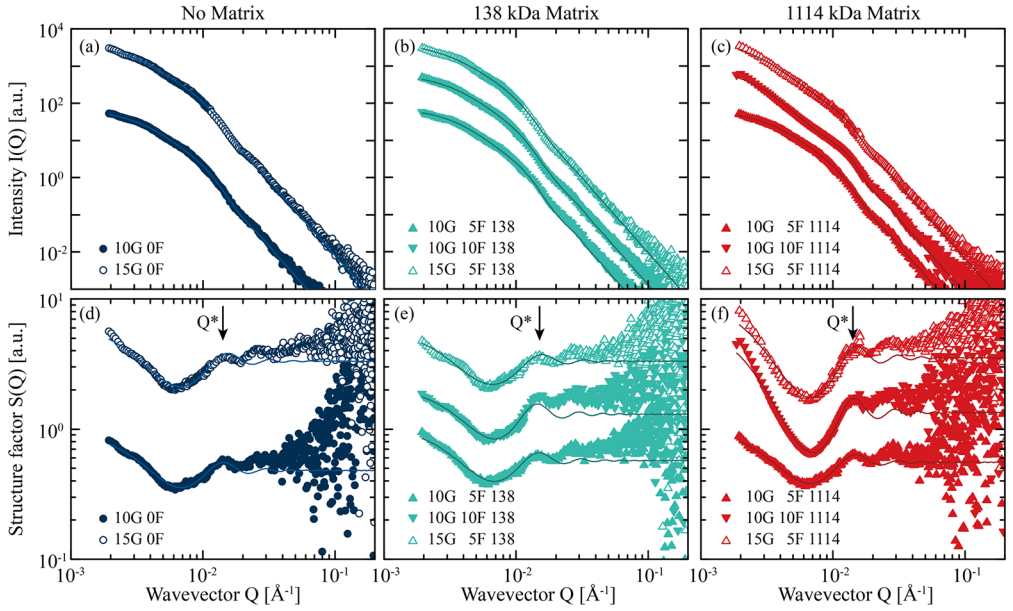

Figure 2. SAXS scattering intensity $I(Q)$ as a function of wavevector Q for polymer-grafted nanoparticles dispersed in (a) neat solvent and in semidilute solutions of polystyrene with M_w of (b) 138 kDa and (c) 1114 kDa. (b) Structure factor $S(Q) = I(Q)/P(Q)$ as a function of wavevector Q for polymer-grafted nanoparticles dispersed in (d) neat solvent and in semidilute solutions of polystyrene with M_w of (e) 138 kDa and (f) 1114 kDa. Data shifted vertically for clarity. Arrows indicate primary peak in $S(Q)$ at Q^*. Solid curves show best fits to eq 1.

images per sample over a 4 × 4 grid with an offset of 4 μm center-to-center distance between images (Supporting Information).

Neutron Spin Echo. The polymer-grafted nanoparticles are suspended in d_5-2-butanone with appropriate amounts of linear d_3-PS (M_W = 138 and 1114 kDa) and homogenized for 3−4 days. We suspend polymer-grafted nanoparticles at a volume fraction of $\phi = 0.1$ in linear matrix polymer at volume fractions of $\phi_M = 0.05$ and 0.1 and at $\phi = 0.15$ in the presence of linear polymer at $\phi_M = 0.05$. Samples are labeled by their percent grafted polymer (G), percent free polymer (F), and the free polymer molecular weight; e.g., 10G 5F 1114 implies $\phi = 0.1$, $\phi_M = 0.05$, and M_w = 1114 kDa linear PS. We measure the dynamics of the grafted polymer using neutron spin echo (NSE) spectroscopy on the BL-15 beamline[30] at the Spallation Neutron Source, Oak Ridge National Laboratory (ORNL). The neutron scattering length densities in 10^{-6} Å^{-2} are 3.277, 3.475, and 3.667 for d_3-PS, SiO_2, and d_5-2-butanone, respectively, and 1.399 for the protonated grafted PS. Thus, the dominant scattering contrast is between the grafted hPS and the solvent,[31] so that the NSE signal is dominated by the relaxation of the grafted hPS (Figure 1b). The NSE data are corrected for incoherent background echoes and instrumental resolution using graphite foil and reduced manually. To check the manual reduction, we also collected data on the NSE beamline at the Center for Neutron Research, National Institute of Standards and Technology (NIST). The NIST data are reduced using the Dave software package[32] and support the manual reduction of the ORNL data (Supporting Information). The samples remained stable in the NSE sample holders with no signs of evaporation over the 2 week duration of the neutron experiments.

RESULTS AND DISCUSSION

Using small-angle neutron scattering (SANS), we measure the structure of the grafted nanoparticles dispersed in d_5-2-butanone (Figure 1b). Because the solvent contrast matches the silica core, the scattering is dominated by the grafted polymer at high Q. On these length scales ($QR_{g,0} > 1$), SANS probes the correlations between the grafted chains similar to a semidilute solution so that the scattering intensity follows a Lorentzian as $I_{coh}(Q) = A/(1 + (Q\xi)^{1/\nu})$, where A is a scaling factor, $\xi = 5.3 \pm 0.4$ nm is the correlation length between polymer chains, and $\nu = 0.47 \pm 0.03$ is the inverse of the polymer fractal dimension. The upturn at low Q is caused by larger scale structures and is not discussed further here.

To measure the dispersion of these particles, we use small-angle X-ray scattering (SAXS) (Figure 2). The X-ray scattering is dominated by the silica cores. At high Q, we observe the classical Q^{-4} scaling for hard spheres. At low Q, however, the SAXS intensity does not plateau, indicating that the particles form some structure at long length scales. To capture this behavior at low Q, we use a fitting form that multiplies the form factor $P(Q)$ by a shift factor A and the sum of a hard-sphere structure factor[33] $S_{HS}(Q)$ and a mass fractal structure factor $S_{MF}(Q)$ (eq 1).

$$I(Q) = AP(Q)[S_{HS}(Q) + S_{MF}(Q)] \quad (1)$$

The hard-sphere form factor for a sphere of radius R is given by

$$P(Q) = \left(\frac{\sin(QR) - QR\cos(QR)}{(QR)^3}\right)^2 \quad (2)$$

and the mass fractal structure factor[34] is given as

$$S_{MF}(Q) = \frac{\Gamma(D_m - 1)\xi_{MF}^{D_m - 1}}{[1 + (Q\xi_{MF})^2]^{(D_m - 1)/2}} \frac{\sin[(D_m - 1)\tan^{-1}(Q\xi_{MF})]}{Q} \quad (3)$$

$S_{MF}(Q)$ captures the scattering intensity for aggregates with a fractal dimension D_m and a correlation length ξ_{MF}, whereas $S_{HS}(Q)$ captures the interparticle scattering within the aggregate.

Fitting the scattering intensity to eq 1, we quantify the interparticle distance within an aggregate and the overall size of the aggregates. The primary peaks at Q^* that appear in the measured $S(Q)$ (Figure 2d−f) indicate that the particles aggregate with a set interparticle spacing $x_{ID} = 2\pi/Q^*$ of approximately 42.5 nm at all matrix concentrations. This interparticle distance is comparable to the average diameter $2R_{NP}$ = 48 nm of the silica cores. For samples without matrix

DOI: 10.1021/acs.macromol.7b01245
Macromolecules 2017, 50, 7372−7379

polymer or with low-M_w matrix (Figure 2d,e), there is a second correlation feature at 0.003 Å^{-1} < Q < 0.004 Å^{-1}, corresponding to length scales of 150−210 nm, which disappears when the particles aggregate in the high-M_w samples (Figure 2f). Because the polymer-grafted nanoparticles have a hydrodynamic radius $R_{H,NP}$ of 68 nm (Supporting Information), we attribute this low-Q feature to the distance between well-dispersed polymer-grafted nanoparticles. Unlike previous work,[35] the low volume fractions of SiO_2 and the polydispersity of the particles used in this study smear the correlation between well-dispersed grafted nanoparticles, making direct quantitative measurements of the size of the polymer-grafted nanoparticles difficult. At low Q, the mass-fractal contribution indicates that the spheres form finite-sized aggregates with a radius of gyration[36] $R_{g,MF} = \sqrt{\xi_{MF}^2 D_m(D_m + 1)/2}$ (Figure 3a). The aggregates are small with $R_{g,MF} \approx 50$ nm at low concentrations of matrix polymers and grow in size to ≈100 nm at high matrix concentration.

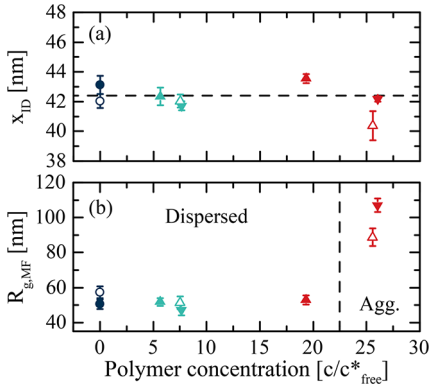

Figure 3. (a) Interparticle distance x_{ID} within aggregates as a function of polymer concentration. Dashed line indicates $x_{ID} \approx 42.5$ nm. (b) Aggregate radius $R_{g,MF}$ as a function of polymer concentration. Dashed line indicates approximate boundary between dispersed and aggregated samples. Symbols same as in Figure 2.

To confirm the presence of large aggregates, we conduct atomic force microscopy (AFM) experiments on thin films of these composites (Figure 4). The solvent is evaporated quickly on time scales less than 5 s to preserve the solution structure. The observed structures qualitatively match those seen in SAXS. At low matrix concentrations, the aggregates are small, contain few particles, and are relatively rare (Figure 4a). At high matrix concentrations, the aggregates are significantly larger, contain more particles, and are abundant (Figure 4b). This aggregation process stands in stark contrast to the autophobic dewetting observed for polymer-grafted nanoparticles dispersed in melts of linear polymer, in which dispersion is controlled by the ratio of grafted and matrix molecular weights.[15]

Instead, aggregation at high matrix concentrations is reminiscent of the structural change in solutions of star and linear polymers caused by an increase in the solution osmotic pressure. For star polymers and other soft colloids, compression and aggregation in solution are separate phenomena. Similarly, dewetting and aggregation are distinct transitions for polymer-grafted particles dispersed in chemically dissimilar polymer matrices due to competing entropic and enthalpic interactions.[17] At low concentrations, linear polymers do not penetrate the star polymers but increase the osmotic pressure to compress the star polymers.[19] At higher

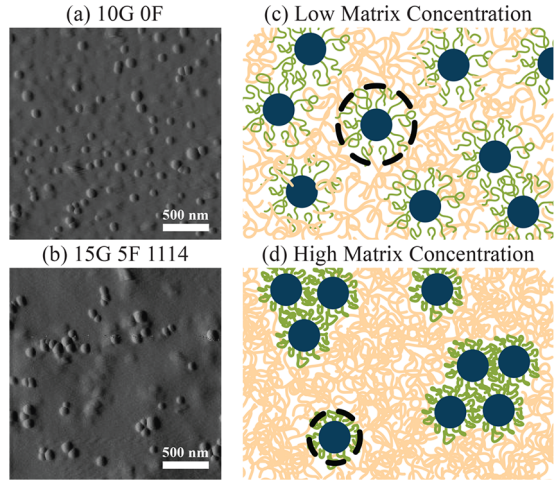

Figure 4. AFM images collected in deflection mode for samples (a) 10G 0F and (b) 15G 5F 1114 show different morphologies. Schematic of solution structure for (c) low $\phi_M \approx 0.05$ and (d) high $\phi_M \approx 0.1$ concentrations of matrix polymer. Dashed circles indicate size of an individual polymer-grafted nanoparticle.

concentrations of linear polymer ($c > c^*$), the star polymers aggregate due to depletion attractions,[20−22] which increase in strength as the size ratio of star to free polymer decreases.[23,24] The same physics governing star polymer morphology applies to dispersions of polymer grafted nanoparticles in linear polymer solutions. The structural change seen in our system, i.e., large clusters at high concentrations of high molecular weight matrix, is qualitatively consistent with the star polymer phase diagram[20] but occurs at higher concentrations of linear polymer ($c \approx (20-25)c^*_{free}$). The shift in phase boundary may be caused by the finite-sized core in a polymer-grafted nanoparticle. Thus, the aggregation of the polymer-grafted nanoparticles at high matrix concentration indicates that the linear polymer does not penetrate the grafted corona but instead compresses the grafted chains and leads to eventual aggregation, as shown schematically in Figure 4c,d. At low matrix concentrations and low M_w, the grafted corona is extended and the particles are well-dispersed. At high matrix concentrations and high M_w, the grafted corona collapses and the particles aggregate.

Given the dramatic change in structure, polymer-grafted nanoparticles dispersed in a semidilute solution of linear polymer is an ideal system to investigate the dynamics of grafted polymer as the grafted corona compresses in a complex fluid. To investigate the dynamics of the grafted polymer, we measure the dynamic correlation function $S(Q,t)$ using NSE over a wavevector range 0.04 Å^{-1} < Q < 0.11 Å^{-1} ($QR_g \gg 1$) and time scales of 0.03 ns < t < 50 ns (Figure 5). Over this wavevector range, the scattering intensity is dominated by the grafted polymer (Figure 1b). With $R_{H,NP}$ = 68 nm, the polymer-grafted nanoparticles are effectively immobile over these time scales, and thus the center-of-mass diffusion does not contribute to $S(Q,t)$. Previous work used a breathing mode analysis[37,38] to fit the relaxations of polymer absorbed to an interface[39] or in micelles[40] in which the grafting density is high (σ > 0.15 chains/nm^2), and $M_w \approx 10$ kDa is low. For lower grafting densities, the breathing mode analysis is no longer appropriate and Zimm relaxations dominate.[41] Because σ = 0.054 ± 0.015 chains/nm^2 and the grafted M_w = 355 kDa is

DOI: 10.1021/acs.macromol.7b01245
Macromolecules 2017, 50, 7372−7379

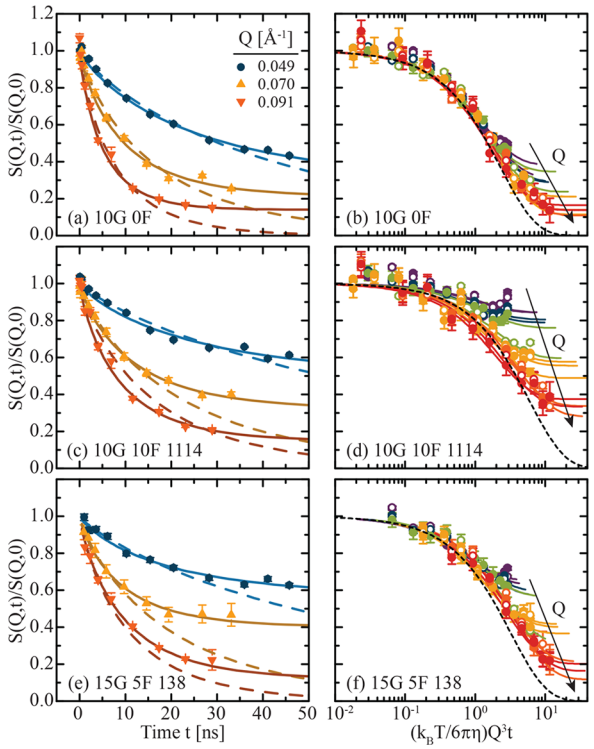

Figure 5. (left) Representative normalized dynamic correlation functions $S(Q,t)/S(Q,0)$ as a function of time t and (right) Zimm scaling plots for samples (a, b) 10G 0F, (c, d) 10G 5F 1114, and (e, f) 15G 5F 138 over a wavevector range of 0.42 Å^{-1} ≤ Q ≤ 0.107 Å^{-1}. Dashed curves are best fits to an initial Zimm decay at short times. Solid curves are best fits to eq 4. Data collected at ORNL with a maximum time of ≈50 ns that depends on Q, neutron wavelength, and instrumental resolution.

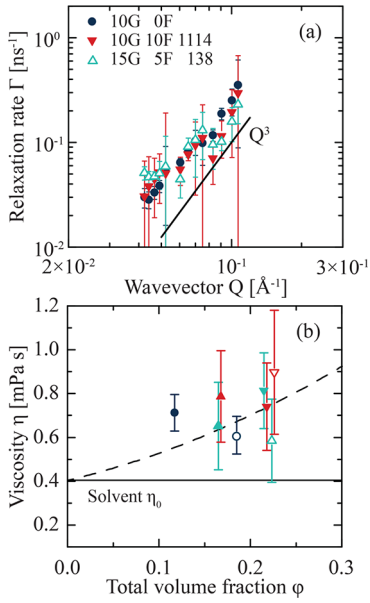

Figure 6. (a) Relaxation rate Γ as a function of wavevector Q for representative solutions. Solid line shows Q^3 scaling. (b) Viscosity η experienced by grafted chains as a function of total volume fraction ϕ. The solid line indicates solvent viscosity, and the dashed line is the Einstein−Batchelor prediction. Symbols same as in Figure 2.

high for our polymer-grafted nanoparticles, we expect to observe Zimm relaxations.

For a free polymer, intrachain relaxations follow the Zimm model with $S(Q,t)/S(Q,0) = \exp[-(\Gamma t)^{0.85}]$,[42] where $\Gamma = (k_BT/6\pi\eta)Q^3$. We find good agreement between this model and the measured relaxations at short times (Figure 5) but observe significant and systematic deviations at long times for all samples, indicating that the grafted polymers relax more slowly than free chains. Previous experiments using dielectric spectroscopy on a self-suspending system of polymer-grafted nanoparticles found the relaxations of the grafted polymer on time scales greater than 1 ms are orders of magnitude slower than for free polymer, which the authors attributed to confinement between chains.[43] We incorporate this proposed confinement into the Zimm model by fitting to a stretched exponential with a long-time plateau

$$S(Q,t) = (1-f)\exp[-(\Gamma t)^{0.85}] + f \quad (4)$$

Long-time plateaus are commonly observed when the material cannot fully relax over the experimental time scale due to crowding or confinement.[44,45] Using this model, we better capture the decay of $S(Q,t)$ at long times (Figure 5).

The relaxation rates Γ extracted from the confined Zimm fits scale as Q^3, in agreement with the Zimm theory (Figure 6a). These relaxation rates correspond to the short time dynamics of the grafted polymer and thus do not exhibit the dynamic crossover from Zimm relaxations to collective diffusion observed in semidilute solutions of free polymer.[46] From the relaxation rates, we calculate the effective viscosity acting on the grafted polymer chain from $\eta = k_BTQ^3/6\pi\Gamma$. On the time and length scales probed by NSE, the viscosity acting over ξ in dilute solutions is not a bulk solution viscosity[42,47] but related to the solvent viscosity η_0 = 4.05 mPa·s. For the semidilute solutions measured here, the effective viscosity is predicted to follow the Einstein−Batchelor expression[48,49] $\eta = \eta_0(1 + 2.5\phi + 6.2\phi^2)$, in good agreement with the measured viscosity (Figure 6b). The agreement between the Einstein−Batchelor prediction and the measured viscosities indicate that the short-time dynamics of the grafted chains are controlled by hydrodynamic interactions and are similar to the relaxations of free polymer.

On longer time scales, however, the neighboring chains begin to affect the grafted chain relaxations. The long-time plateaus in $S(Q,t)$ indicate that the polymer cannot fully relax within the experimental time scale. Because the dynamic correlation function is related to displacement via $S(Q,t)/S(Q,0) = \exp(-\langle\Delta r^2\rangle Q^2/6)$,[50] we calculate the length scale L over which the grafted chains are confined according to $f = \exp(-(LQ)^2/6)$ (Figure 7a). We expect the polymer to be confined over the distance between grafted chains, which is calculated from the grafting density as $L = \sqrt{4/\pi\sigma_G} = 4.9$ nm at the particle surface. Because of the curvature of the nanoparticle, the grafting density decreases away from the particle surface, resulting in $L \approx 9$ nm at 25 nm away from the particle surface. Nevertheless, this estimate of the confinement length at the particle surface agrees with the measured confinement length in the absence of linear polymer within experimental error (Figure 7b). For a free polymer undergoing Zimm relaxations, the monomer mean-squared displacement is given by[46]

$$\langle\Delta r^2(t)\rangle = \frac{16}{9\pi^{3/2}}\left(\frac{\sqrt{3\pi}k_BTt}{\eta_0}\right)^{2/3} \quad (5)$$

DOI: 10.1021/acs.macromol.7b01245
Macromolecules 2017, 50, 7372−7379

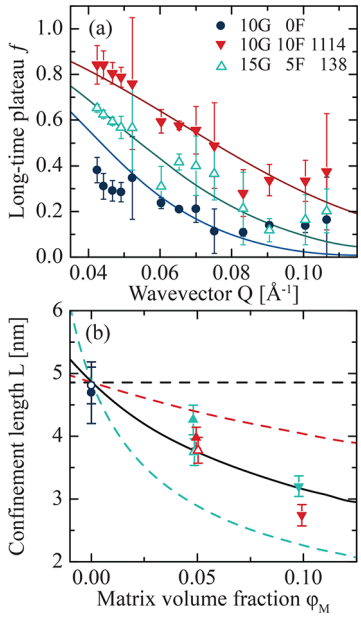

Figure 7. (a) Long time plateau f of $S(Q,t)$ as a function of wavevector Q for representative solutions. Solid curves are fits to confinement length model. (b) Confinement length L as a function of matrix volume fraction ϕ_M. Dashed black line shows prediction in the absence of linear polymer. Dashed teal and red curves are predictions for fully penetrating linear polymer at low and high matrix M_w, respectively. Solid curve is prediction for nonpenetrating matrix. Symbols same as in Figure 2.

Using eq 5 and the parameters of our experiments (T = 298 K, η_0 = 0.405 mPa·s, and a maximum measurement time of $t \approx 50$ ns), we calculate the expected monomer displacement for a free chain to be $\langle \Delta r \rangle \approx 6.6$ nm, greater than the measured confinement of 4.9 nm in the absence of matrix polymer. At high matrix concentrations with the maximum measured viscosity of $\eta \approx 0.9$ mPa·s (Figure 6b), the monomer displacement of a free chain is expected to be 5 nm, which is again greater than the measured confinement of 3.8 nm (Figure 7b). This difference between the measured confinement length and the predicted displacement for a free chain emphasizes the unique dynamics of grafted polymer. Although such a confining length scale has been proposed to explain slow relaxations of grafted polymer,[43] it has not been previously measured, to the best of our knowledge.

The experimentally measured confinement length decreases with increasing polymer matrix concentration (Figure 7b). To understand this dependence, we note that the compressed corona has a higher local concentration of grafted chains. The higher concentration of grafted chains results in an effective grafting density $\sigma_M = \phi_M \rho_M N_A / M_w a$, where a is the specific particle surface area per solution volume and M_w is the molecular weight of the grafted chains. By increasing the effective grafting density, the addition of nonpenetrating matrix chains leads to a decrease in the confinement length via $L = \sqrt{4/\pi(\sigma_G + \sigma_M)}$ (solid curve in Figure 7b). Without any fitting parameters, this prediction agrees well with our measurements. In contrast, for penetrating chains, we would expect the effective grafting density to depend on the matrix M_w (dashed curves in Figure 7b), which is not observed for our data. Thus, the compression of the grafted corona in the presence of linear free chains leads to an increase in confinement of the grafted chains, in agreement with the previously observed structural changes.

The interactions between grafted nanoparticles and free chains underlying the structural and dynamical changes of the polymer-grafted nanoparticles are complex, likely dependent on the size ratio between polymer-grafted nanoparticles and the free polymer, the polymer grafting density, and the particle curvature. Our experiments span size ratios of $1.5 < R_{H,NP}/R_{g,0} < 5.5$, where osmotic pressure strongly affects the structure of the grafted nanoparticles.[20,23,24] The limits for these interactions are likely similar to those for mixtures of star and linear polymers. For smaller size ratios, the linear polymer becomes larger than the grafted nanoparticle, and the depletion model no longer holds.[24] For larger size ratios, the free polymer is much smaller than the grafted particle and would penetrate the grafted corona, leading to weak interactions.[21] Further, the confined dynamics depend strongly on the grafting density of the particle. For lower grafting densities, we expect the grafted polymer to no longer be confined, especially as the predicted confinement length approaches the radius of gyration of the grafted polymer. For much higher grafting densities, the grafted polymer should relax through collective breathing modes.[40] Finally, the curvature of the particle affects how the grafted polymer density varies in the radial direction.[51] For relatively large particles similar to the ones used in this study, the density profile gradually changes away from the particle surface so that the confinement length agrees with the surface grafting density. For smaller particles with larger curvature, the polymer density profile will be steeper so that the confinement length may deviate from predictions using the surface grafting density. The effect of these various parameters on the dynamics of grafted polymer is incompletely understood and should be the focus of further study.

CONCLUSION

Polymer-grafted nanoparticles are well-dispersed in solutions of linear polymer at low matrix concentrations but aggregate at high matrix concentrations due to the compression of the grafted chains and resulting depletion interactions. The rich structural behavior of these starlike grafted particles makes this an ideal system to directly measure the dynamics of grafted polymer in complex fluids. On short time scales, the grafted polymer chains relax according to the Zimm model. On longer time scales, the polymer chains are confined by neighboring chains. Our work presents direct empirical evidence of a confinement length scale to explain the previously measured slow dynamics of grafted polymers. In the presence of free linear polymer, the grafted polymers compress and become more confined with a decrease in the confinement length. We attribute this behavior to an increase in an effective grafting density.

By directly measuring the confinement of grafted polymer relaxations, we generate new scientific understanding that will be significant for a wide variety of applications requiring the dispersion of polymer-grafted particles in complex media. Structurally, controlling the phase behavior of grafted particles in solutions may lead to better solvent processing methods to create dispersed polymer composites.[52,53] Additionally, this work raises an important question: how the confined dynamics of the grafted polymer affect the bulk mechanical properties of composite solutions and melts. Beyond composites, grafted particles are commonly used in a variety of fields, such as targeted drug delivery[54,55] in which the dynamics of the grafted

DOI: 10.1021/acs.macromol.7b01245
Macromolecules 2017, 50, 7372−7379

polymer may affect the release profile of a drug. These particles are often dispersed in complex media, such as blood or the cellular cytoplasm,[56,57] which contain a distribution of particles of varying size, surface chemistry, and charge, all of which could affect the structure and dynamics of the grafted polymer beyond a simple increase in osmotic pressure. Nevertheless, relating structural changes (e.g., confinement) to dynamic signatures (e.g., slow relaxations) will generate insight into how the local environment affect the performance and efficacy of the grafted particles.

■ ASSOCIATED CONTENT

Supporting Information

The Supporting Information is available free of charge on the ACS Publications website at DOI: 10.1021/acs.macromol.7b01245.

Details of sample preparation, dynamic light scattering results, discussion of normalization procedure for NSE data collected at ORNL, comparison of fitting forms, plots of relaxation rates and long-time plateaus for all samples, and discussion of AFM experiments (PDF)

■ AUTHOR INFORMATION

Corresponding Authors

*E-mail: jcconrad@uh.edu (J.C.C.).
*E-mail: ramanan@uh.edu (R.K.).

ORCID

Ryan Poling-Skutvik: 0000-0002-1614-1647
Jacinta C. Conrad: 0000-0001-6084-4772
Ramanan Krishnamoorti: 0000-0001-5831-502X

Notes

The authors declare no competing financial interest.

■ ACKNOWLEDGMENTS

We thank Adeline Mah for help preparing AFM samples, Lisa Liu for suggestions on NSE analysis and many helpful discussions, Dr. Peter Vekilov for access to the AFM instrument, and Dr. Kevin Weiss at SNS for help preparing NSE samples. This research used resources of the Advanced Photon Source, a U.S. Department of Energy (DOE) Office of Science User Facility operated for the DOE Office of Science by Argonne National Laboratory under Contract DE-AC02-06CH11357. This research at the BL-15 NSE beamline at Oak Ridge National Lab's Spallation Neutron Source was sponsored by the Scientific User Facilities Division, Office of Basic Energy Sciences, DOE. This work utilized the NIST Center for Neutron Research (NCNR) supported in part by the National Science Foundation (NSF) under Agreement DMR-1508249. The SAXS experiments at UH were performed on an instrument obtained on an NSF grant (NSF DMR 1040446). R.K. acknowledges funding from ExxonMobil Company. J.C.C. acknowledges funding from NSF (CBET-1438204) and the Welch Foundation (E-1869).

■ ADDITIONAL NOTE

[a]The identification of any commercial product or trade name does not imply endorsement or recommendation by the National Institute of Standards and Technology.

■ REFERENCES

(1) Chevigny, C.; Dalmas, F.; Di Cola, E.; Gigmes, D.; Bertin, D.; Boué, F.; Jestin, J. Polymer-grafted-nanoparticles nanocomposites: Dispersion, grafted chain conformation, and rheological behavior. *Macromolecules* **2011**, *44*, 122−133.

(2) Black, K. C. L.; Wang, Y.; Luehmann, H. P.; Cai, X.; Xing, W.; Pang, B.; Zhao, Y.; Cutler, C. S.; Wang, L. V.; Liu, Y.; Xia, Y. Radioactive ^{198}Au-doped nanostructures with different shapes for in vivo analyses of their biodistribution, tumor uptake, and intratumoral distribution. *ACS Nano* **2014**, *8*, 4385−4394.

(3) Howes, P. D.; Chandrawati, R.; Stevens, M. M. Colloidal nanoparticles as advanced biological sensors. *Science* **2014**, *346*, 1247390.

(4) Lo Verso, F.; Yelash, L.; Binder, K. Dynamics of macromolecules grafted in spherical brushes under good solvent conditions. *Macromolecules* **2013**, *46*, 4716−4722.

(5) Rubinstein, M.; Colby, R. H. *Polymer Physics*; Oxford University Press: New York, 2003.

(6) Klushin, L. I.; Skvortsov, A. M. Critical dynamics of a polymer chain in a grafted monolayer. *Macromolecules* **1991**, *24*, 1549−1553.

(7) Lang, M.; Werner, M.; Dockhorn, R.; Kreer, T. Arm Retraction Dynamics in Dense Polymer Brushes. *Macromolecules* **2016**, *49*, 5190−5201.

(8) Fytas, G.; Anastasiadis, S.; Seghrouchni, R.; Vlassopoulos, D.; Li, J.; Factor, B.; Theobald, W.; Toprakcioglu, C. Probing Collective Motions of Terminally Anchored Polymers. *Science* **1996**, *274*, 2041−2044.

(9) Yakubov, G. E.; Loppinet, B.; Zhang, H.; Rühe, J.; Sigel, R.; Fytas, G. Collective Dynamics of an End-Grafted Polymer Brush in Solvents of Varying Quality. *Phys. Rev. Lett.* **2004**, *92*, 115501.

(10) Michailidou, V. N.; Loppinet, B.; Prucker, O.; Rühe, J.; Fytas, G. Cooperative Diffusion of End-Grafted Polymer Brushes in Good Solvents. *Macromolecules* **2005**, *38*, 8960−8962.

(11) Michailidou, V. N.; Loppinet, B.; Vo, D. C.; Prucker, O.; Rühe, J.; Fytas, G. Dynamics of end-grafted polystyrene brushes in theta solvents. *J. Polym. Sci., Part B: Polym. Phys.* **2006**, *44*, 3590−3597.

(12) Reith, D.; Milchev, A.; Virnau, P.; Binder, K. Computer simulation studies of chain dynamics in polymer brushes. *Macromolecules* **2012**, *45*, 4381−4393.

(13) Akcora, P.; Liu, H.; Kumar, S. K.; Moll, J.; Li, Y.; Benicewicz, B. C.; Schadler, L. S.; Acehan, D.; Panagiotopoulos, A. Z.; Pryamitsyn, V.; Ganesan, V.; Ilavsky, J.; Thiyagarajan, P.; Colby, R. H.; Douglas, J. F. Anisotropic self-assembly of spherical polymer-grafted nanoparticles. *Nat. Mater.* **2009**, *8*, 354−359.

(14) Goel, V.; Pietrasik, J.; Dong, H.; Sharma, J.; Matyjaszewski, K.; Krishnamoorti, R. Structure of Polymer Tethered Highly Grafted Nanoparticles. *Macromolecules* **2011**, *44*, 8129−8135.

(15) Kumar, S. K.; Jouault, N.; Benicewicz, B.; Neely, T. Nanocomposites with polymer grafted nanoparticles. *Macromolecules* **2013**, *46*, 3199−3214.

(16) Dang, A.; Ojha, S.; Hui, C. M.; Mahoney, C.; Matyjaszewski, K.; Bockstaller, M. R. High-transparency polymer nanocomposites enabled by polymer-graft modification of particle fillers. *Langmuir* **2014**, *30*, 14434−14442.

(17) Martin, T. B.; Mongcopa, K. I. S.; Ashkar, R.; Butler, P.; Krishnamoorti, R.; Jayaraman, A. Wetting-Dewetting and Dispersion-Aggregation Transitions Are Distinct for Polymer Grafted Nanoparticles in Chemically Dissimilar Polymer Matrix. *J. Am. Chem. Soc.* **2015**, *137*, 10624−10631.

(18) Holt, A. P.; et al. Controlling interfacial dynamics: covalent bonding versus physical adsorption in polymer nanocomposites. *ACS Nano* **2016**, *10*, 6843−6852.

(19) Wilk, A.; Huißmann, S.; Stiakakis, E.; Kohlbrecher, J.; Vlassopoulos, D.; Likos, C. N.; Meier, G.; Dhont, J. K. G.; Petekidis, G.; Vavrin, R. Osmotic shrinkage in star/linear polymer mixtures. *Eur. Phys. J. E: Soft Matter Biol. Phys.* **2010**, *32*, 127−134.

(20) Stiakakis, E.; Petekidis, G.; Vlassopoulos, D.; Likos, C. N.; Iatrou, H.; Hadjichristidis, N.; Roovers, J. Depletion and cluster

DOI: 10.1021/acs.macromol.7b01245
Macromolecules 2017, 50, 7372−7379

formation in soft colloid-polymer mixtures. *Eur. Lett.* **2005**, *72*, 664−670.
(21) Camargo, M.; Likos, C. N. Unusual features of depletion interactions in soft polymer-based colloids mixed with linear homopolymers. *Phys. Rev. Lett.* **2010**, *104*, 078301.
(22) Camargo, M.; Egorov, S. A.; Likos, C. N. Cluster formation in star-linear polymer mixtures: equilibrium and dynamical properties. *Soft Matter* **2012**, *8*, 4177.
(23) Vlassopoulos, D. Colloidal star polymers: Models for studying dynamically arrested states in soft matter. *J. Polym. Sci., Part B: Polym. Phys.* **2004**, *42*, 2931−2941.
(24) Stiakakis, E.; Vlassopoulos, D.; Likos, C. N.; Roovers, J.; Meier, G. Polymer-mediated melting in ultrasoft colloidal gels. *Phys. Rev. Lett.* **2002**, *89*, 208302.
(25) Penn, L. S.; Hunter, T. F.; Lee, Y.; Quirk, R. P. Grafting Rates of Amine-Functionalized Polystyrenes onto Epoxidized Silica Surfaces. *Macromolecules* **2000**, *33*, 1105−1107.
(26) Qin, S.; Qin, D.; Ford, W. T.; Resasco, D. E.; Herrera, J. E. Functionalization of Single-Walled Carbon Nanotubes with Polystyrene via Grafting to and Grafting from Methods. *Macromolecules* **2004**, *37*, 752−757.
(27) Balazs, A. C.; Emrick, T.; Russell, T. P. Nanoparticle Polymer Composites: Meet Two Small Worlds. *Science* **2006**, *314*, 1107−1110.
(28) Wagner, H. L. The Mark-Houwink-Sakurada Equation for the Viscosity of Atactic Polystyrene. *J. Phys. Chem. Ref. Data* **1985**, *14*, 1101−1106.
(29) Kline, S. R. Reduction and analysis of SANS and USANS data using IGOR Pro. *J. Appl. Crystallogr.* **2006**, *39*, 895−900.
(30) Ohl, M.; et al. The spin-echo spectrometer at the Spallation Neutron Source (SNS). *Nucl. Instrum. Methods Phys. Res., Sect. A* **2012**, *696*, 85−99.
(31) Poling-Skutvik, R.; Mongcopa, K. I. S.; Faraone, A.; Narayanan, S.; Conrad, J. C.; Krishnamoorti, R. Structure and Dynamics of Interacting Nanoparticles in Semidilute Polymer Solutions. *Macromolecules* **2016**, *49*, 6568−6577.
(32) Azuah, R. T.; Kneller, L. R.; Qiu, Y.; Tregenna-Piggott, P. L. W.; Brown, C. M.; Copley, J. R. D.; Dimeo, R. M. DAVE: A Comprehensive Software Suite for the Reduction, Visualization, and Analysis of Low Energy Neutron Spectroscopic Data. *J. Res. Natl. Inst. Stand. Technol.* **2009**, *114*, 341−358.
(33) Percus, J. K.; Yevick, G. J. Analysis of Classical Statistical Mechanics by Means of Collective Coordinates. *Phys. Rev.* **1958**, *110*, 1−13.
(34) Mildner, D. F. R.; Hall, P. L. Small-angle scattering from porous solids with fractal geometry. *J. Phys. D: Appl. Phys.* **1986**, *19*, 1535−1545.
(35) Jiao, Y.; Akcora, P. Understanding the role of grafted polystyrene chain conformation in assembly of magnetic nanoparticles. *Phys. Rev. E* **2014**, *90*, 042601.
(36) Teixeira, J. Small-angle scattering by fractal systems. *J. Appl. Crystallogr.* **1988**, *21*, 781−785.
(37) de Gennes, P.-G. Dynamics of a diffuse layer of adsorbed polymer. *C. R. Acad. Sci., Ser. II* **1986**, *302*, 765−768.
(38) de Gennes, P. G. Polymers at an interface; a simplified view. *Adv. Colloid Interface Sci.* **1987**, *27*, 189−209.
(39) Jiang, N.; Endoh, M. K.; Koga, T.; Masui, T.; Kishimoto, H.; Nagao, M.; Satija, S. K.; Taniguchi, T. Nanostructures and Dynamics of Macromolecules Bound to Attractive Filler Surfaces. *ACS Macro Lett.* **2015**, *4*, 838−842.
(40) Farago, B.; Monkenbusch, M.; Richter, D.; Huang, J. S.; Fetters, L. J.; Gast, A. P. Collective dynamics of tethered chains: Breathing modes. *Phys. Rev. Lett.* **1993**, *71*, 1015−1018.
(41) Kanaya, T.; Monkenbusch, M.; Watanabe, H.; Nagao, M.; Richter, D. Dynamics of deuterated polystyrene-protonated butadiene diblock copolymer micelles by neutron spin echo. *J. Chem. Phys.* **2005**, *122*, 144905.
(42) Richter, D.; Monkenbusch, M.; Arbe, A.; Colmenero, J. *Adv. Polym. Sci.* **2005**, *174*, 1−221, DOI: 10.1007/b106578.
(43) Agarwal, P.; Kim, S. A.; Archer, L. A. Crowded, confined, and frustrated: Dynamics of molecules tethered to nanoparticles. *Phys. Rev. Lett.* **2012**, *109*, 258301.
(44) Van Megen, W.; Underwood, S. M. Dynamic-light-scattering study of glasses of hard colloidal spheres. *Phys. Rev. E.* **1993**, *47*, 248−261.
(45) Frielinghaus, X.; Brodeck, M.; Holderer, O.; Frielinghaus, H. Confined polymer dynamics on clay platelets. *Langmuir* **2010**, *26*, 17444−17448.
(46) Ewen, B.; Richter, D. *Adv. Polym. Sci.* **1997**, *134*, 1−126.
(47) Monkenbusch, M. In *Neutron Spin Echo Spectrosc. Basics, Trends Appl.*; Mezei, F., Pappas, C., Gutberlet, T., Eds.; Springer: 2003; pp 246−265.
(48) Richter, D.; Binder, K.; Ewen, B.; Stuehn, B. Screening of hydrodynamic interactions in dense polymer solutions: a phenomenological theory and neutron-scattering investigations. *J. Phys. Chem.* **1984**, *88*, 6618−6633.
(49) Griffin, P. J.; Bocharova, V.; Middleton, L. R.; Composto, R. J.; Clarke, N.; Schweizer, K. S.; Winey, K. I. Influence of the Bound Polymer Layer on Nanoparticle Diffusion in Polymer Melts. *ACS Macro Lett.* **2016**, *5*, 1141−1145.
(50) Lungova, M.; Krutyeva, M.; Pyckhout-Hintzen, W.; Wischnewski, A.; Monkenbusch, M.; Allgaier, J.; Ohl, M.; Sharp, M.; Richter, D. Nanoscale Motion of Soft Nanoparticles in Unentangled and Entangled Polymer Matrices. *Phys. Rev. Lett.* **2016**, *117*, 147803.
(51) Daoud, M.; Cotton, J. Star shaped polymers: a model for the conformation and its concentration dependence. *J. Phys. (Paris)* **1982**, *43*, 531−538.
(52) Bockstaller, M. R.; Thomas, E. L. Optical Properties of Polymer-Based Photonic Nanocomposite Materials. *J. Phys. Chem. B* **2003**, *107*, 10017−10024.
(53) Tuteja, A.; Duxbury, P. M.; Mackay, M. E. Multifunctional nanocomposites with reduced viscosity. *Macromolecules* **2007**, *40*, 9427−9434.
(54) Nasongkla, N.; Bey, E.; Ren, J.; Ai, H.; Khemtong, C.; Guthi, J. S.; Chin, S. F.; Sherry, A. D.; Boothman, D. A.; Gao, J. Multifunctional polymeric micelles as cancer-targeted, MRI-ultrasensitive drug delivery systems. *Nano Lett.* **2006**, *6*, 2427−2430.
(55) Mura, S.; Nicolas, J.; Couvreur, P. Stimuli-responsive nanocarriers for drug delivery. *Nat. Mater.* **2013**, *12*, 991−1003.
(56) Minton, A. P. Implications of macromolecular crowding for protein assembly. *Curr. Opin. Struct. Biol.* **2000**, *10*, 34−39.
(57) Ulrich Hartl, F.; Hayer-Hartl, M. Molecular Chaperones in the Cytosol: from Nascent Chain to Folded Protein. *Science* **2002**, *295*, 1852−1858.

DOI: 10.1021/acs.macromol.7b01245
Macromolecules 2017, 50, 7372−7379